Materials Research Express

PAPER

Temperature stability of coercivity in mischmetal-Fe-Co-B melt-spun ribbons

To cite this article: Rui Li *et al* 2018 *Mater. Res. Express* **5** 056101

Materials Research Express

PAPER

RECEIVED
6 February 2018

REVISED
11 April 2018

ACCEPTED FOR PUBLICATION
19 April 2018

PUBLISHED
2 May 2018

Temperature stability of coercivity in mischmetal-Fe-Co-B melt-spun ribbons

Rui Li[1,2], Hong-Rui Zhang[1,2], Yao Liu[1,2], Shu-Lan Zuo[1,2], Jie-Fu Xiong[1,2], Wen-Liang Zuo[1,2], Tong-Yun Zhao[1,2], Feng-Xia Hu[1,2], Ji-Rong Sun[1,2] and Bao-Gen Shen[1,2]

1 State Key Laboratory of Magnetism, Institute of Physics, Chinese Academy of Sciences, Beijing 100190, People's Republic of China
2 University of Chinese Academy of Sciences, Beijing 100049, People's Republic of China

E-mail: shenbg@iphy.ac.cn

Keywords: permanent magnets, coercivity thermal-stability, mischmetal-Fe-B, grain size, intergranular exchange coupling

Abstract

Coercivity temperature coefficient (β) of the permanent magnet depends on its intrinsic magnetic properties and microstructure. In this paper, the relationship between β and the temperature stabilities of magnetocrystalline anisotropy field (H_a) and saturation magnetization (M_s) as well as the microstructure is discussed. Regarding two concerned microstructural factors: grain size and grain boundary, coercivity thermal-stabilities of $MM_{13.5}Fe_{79.5}B_7$ (MM-mischmetal: unseparated La-Ce-Pr-Nd alloy) and $MM_xFe_{94-x}B_6$ (x = 12, 13, 14, 15, 16, 19) melt-spun ribbons, respectively, are investigated. High β values near the theoretical limit are obtained either by decreasing grain size or by reducing MM percentage. In addition, coercivities above room temperature of $MM_{13.5}Fe_{79.5-y}Co_yB_7$ (y = 0, 3, 6, 9, 12, 15) melt-spun ribbons are measured. The detailed influences of Co substitutions on β are analyzed, and the weak temperature dependence of M_s is proved to the reason for the observed decrease of β. These findings suggest that proper strategy to minimize local stray fields is the key to enhance coercivity thermal-stability of 2:14:1 structure magnet.

1. Introduction

$Nd_2Fe_{14}B$ magnets have been widely employed into various applications due to their excellent magnetic properties of high induction and coercivity (H_c). In practice, permanent magnets are not merely used at room temperature, their related devices often work at high temperature, even to 200 °C. Coercivity temperature-sensitive characteristic of $Nd_2Fe_{14}B$ thus limits its application at elevated temperature [1–4]. Hence, to improve coercivity temperature-stability in $Nd_2Fe_{14}B$ magnets has been researched as a topic of great interest. Coercivity thermal-stability of magnet is evaluated by the temperature coefficient of coercivity (β): $\beta = [H_c(T_1) - H_c(T_0)]/[H_c(T_0) \cdot (T_1 - T_0)]$, where T_1 is elevated temperature and T_0 is room temperature. To obtain high β value, $Nd_2Fe_{14}B$ magnets are usually replaced by heavy rare-earth Dy, because Dy atoms partially substituting into Nd sites could be able to compensate the large negative magnetocrystalline anisotropy field (H_a) temperature coefficient of $Nd_2Fe_{14}B$ [5]. Another interesting finding is that Y, La or Ce additions in $Nd_2Fe_{14}B$ magnets are beneficial to the temperature stability of coercivity [6–8]. Unlike Dy-doped magnets, high β values in Y, La, Ce-containing magnets are attributed to their enhanced temperature stabilities of H_a resulting from the weak temperature dependence of H_a in $Y_2Fe_{14}B$, $La_2Fe_{14}B$ and $Ce_2Fe_{14}B$ [9]. Besides the temperature stability of H_a, changes in microstructure of magnet can also affect the temperature stability of coercivity. Grain refinement and grain boundary modification, such as doping Al, Ga, Nb, Zr, Mo, Hf, etc [10–13] or diffusing Nd(Pr)-Cu and Nd(Pr)-Al [14–17] in $Nd_2Fe_{14}B$ magnets, have been attempted to increase the value of β. Similar to the factors affecting H_c [18], the intrinsic magnetic properties and the microstructure of magnet together determine β. However, few studies have been focused on establishing the relationship between β and its influencing factors. The enhancement mechanism of coercivity thermal-stability is still not fully understood.

In this article, a formula describing the dependences of β on the intrinsic magnetic properties and microstructure is derived from the coercivity micromagnetic equation. With the formula, the effects of grain size and grain boundary on β are analyzed in $MM_{13.5}Fe_{79.5}B_7$ (MM-mischmetal: unseparated La-Ce-Pr-Nd alloy) and $MM_xFe_{94-x}B_6$ (x = 12, 13, 14, 15, 16, 19) melt-spun ribbons, respectively. In addition, the detailed influences of Co substitutions on β in $MM_{13.5}Fe_{79.5-y}Co_yB_7$ (y = 0, 3, 6, 9, 12, 15) melt-spun ribbons are investigated. These researches would serve as a reference for the design and preparation of high thermal-stability permanent magnets.

2. Experiment

Alloy ingots with nominal compositions of $MM_xFe_{94-x}B_6$ (x = 12, 13, 14, 15, 16, 19) and $MM_{13.5}Fe_{79.5-y}Co_yB_7$ (y = 0, 3, 6, 9, 12, 15) are fabricated by arc melting 99.9% Fe, 99.9% Co, 99.9% Nd, 99.7% MM and 97% FeB under the protection of Ar atmosphere. The MM alloy consists of 28.3 wt% La, 50.5 wt% Ce, 5.2 wt% Pr, 15.7 wt% Nd and 0.3 wt% others. The ribbons are produced by induction melting the ingot in quartz tubes and then ejected onto the surface of a rotating copper wheel under argon. The optimum wheel surface velocity ranges from 20 m s^{-1} to 25 m s^{-1}. The $MM_{13.5}Fe_{79.5}B_7$ ribbons with different grain sizes are obtained at the wheel speed of 5 m/s, 10 m s^{-1}, 15 m s^{-1} and 20 m s^{-1}, respectively. Then the wheel sides of the ribbons are polished to improve the homogeneity of grain size distribution, finally the ribbons possess thickness of about 10 μm. The $MM_{13.5}Fe_{79.5}B_7$ ingot is annealed at 1223 K for one week and then crushed to powders with particle size smaller than 30 μm. The powders mixing with epoxy resin are fabricated into an anisotropic magnet by aligning in a magnetic field.

Grain size of the $MM_{13.5}Fe_{79.5}B_7$ ribbons at different wheel speeds are determined by transmission electron microscopy (TEM) and scanning electron microscope (SEM). Curie temperatures (T_C) for $MM_{13.5}Fe_{79.5-y}Co_yB_7$ are determined by the temperature dependence of magnetization with a vibrating sample magnetometer (VSM) in a magnetic field of 500 Oe. The demagnetization curves of all ribbons are measured by a superconducting quantum interference device (SQUID-VSM) with a magnetic field of up to 70 kOe, from 300 up to 400 K. The magnetization curve perpendicular to the magnetically easy direction of the anisotropic $MM_{13.5}Fe_{79.5}B_7$ magnet is measured and its magnetocrystalline anisotropy fields (H_a) at temperatures are determined by a method of singular point detection (SPD) [19].

3. Results and discussion

Coercivity (H_c) of permanent magnet is known to be much lower than predicted by theory due to the Brown's Paradox, and it could be expressed by a phenomenological micromagnetic model [18, 20]:

$$H_c(T) = aH_a(T) - N_{eff}M_s(T) \tag{1}$$

where M_s(T) and H_a(T) are the temperature dependence of saturation magnetization and magnetocrystalline anisotropy field, respectively. The microstructural parameter *a* describes the influence of the magnetically inhomogeneous defects in grain surface or grain boundary on the crystal anisotropy. The effective demagnetization factor N_{eff} represents the effect of local stray fields determined by the grain size and grain shape as well as the intergranular interactions like the short-range exchange interaction and the long-range stray fields. Temperature coefficient of coercivity (β) is used to evaluate the coercivity thermal-stability of magnet:

$$\beta = \frac{H_c(T_1) - H_c(T_0)}{H_c(T_0)\cdot(T_1 - T_0)} \tag{2}$$

where T_1 is elevated temperature and T_0 is room temperature. Combining (2) with (1), β can be expressed:

$$\beta = \frac{a[H_a(T_1) - H_a(T_0)] - N_{eff}[M_s(T_1) - M_s(T_0)]}{H_c(T_0)\cdot(T_1 - T_0)} \tag{3}$$

after simplification

$$\beta = h + \frac{h - m}{\frac{a}{N_{eff}}\cdot k - 1} \tag{4}$$

where $h = \frac{H_a(T_1) - H_a(T_0)}{H_a(T_0)\cdot(T_1 - T_0)}$, $m = \frac{M_s(T_1) - M_s(T_0)}{M_s(T_0)\cdot(T_1 - T_0)}$, $k = \frac{H_a(T_0)}{M_s(T_0)}$. *h* and *m* represent the temperature coefficient of H_a and M_s, respectively. *k* is the so-called magnetic hardness parameter [21]. Taking into account the relative change rate (Δ) of β to *h*,

$$\Delta = \frac{\beta - h}{h} = \frac{1 - m/h}{\frac{a}{N_{eff}}\cdot k - 1} \tag{5}$$

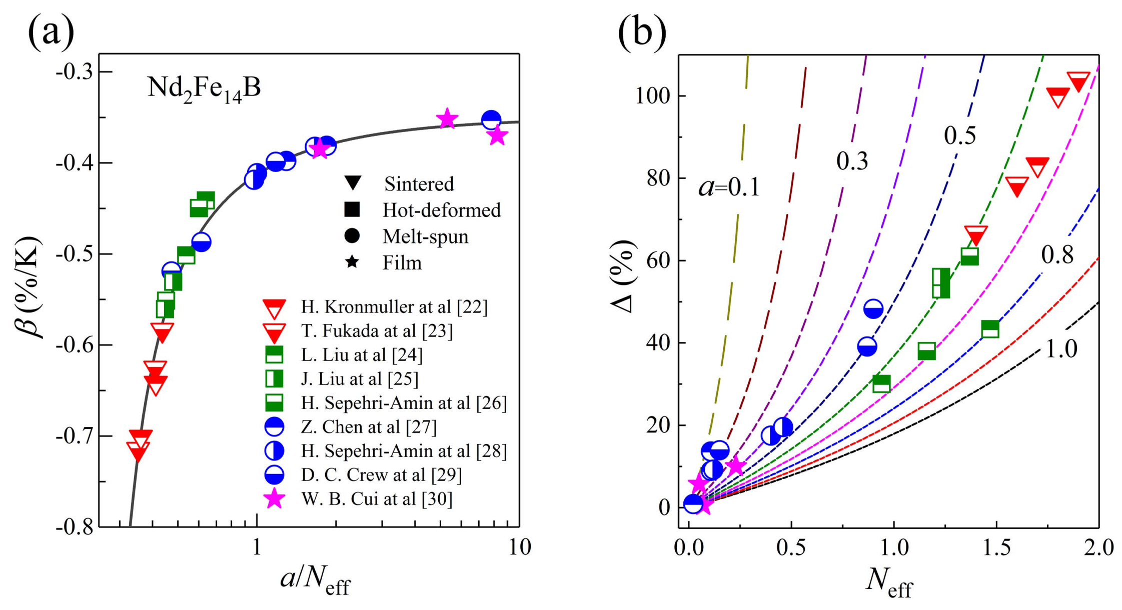

Figure 1. (a) β versus a/N_{eff} for $Nd_2Fe_{14}B$ film, melt-spun, hot-deformed and sintered magnets [22–30] and the curve calculated by equation (4). (b) The curves of $\Delta(N_{eff})$, respectively, for $a = 0.1, 0.2, \ldots, 0.9, 1.0$ calculated by equation (5) and Δ of the magnets in (a) with the corresponding a and N_{eff}.

Table 1. The temperature coefficient of M_s and H_a (m and h), H_a, M_s and the ratio (k) of H_a to M_s at 300 K for $MM_2Fe_{14}B$ and $Nd_2Fe_{14}B$.

Magnet	m (%/K)	h (%/K)	h-m (%/K)	H_a (T)	M_s (T)	k (H_a/M_s)
$MM_2Fe_{14}B$	−0.212	−0.295	−0.083	4.2	1.32	3.2
$Nd_2Fe_{14}B$	−0.124	−0.347	−0.223	7.6	1.61	4.7

β can be also expressed:

$$\beta = h \cdot (1 + \Delta) \tag{6}$$

Essentially, equation (4) is the transformation of equation (1). It could provide a direct understanding of the mechanism of coercivity thermal-stability and relate it to the microstructure of magnet. For example, the dependences of β and Δ in $Nd_2Fe_{14}B$ magnets [22–30] on the microstructural parameters are plotted in figures 1(a) and (b), respectively. From which, we can see that the theoretical upper limit of β equals h due to the absolute value of m is lower than that of h (table 1), and β of $Nd_2Fe_{14}B$ magnets using different techniques roughly decrease from the film and melt-spun magnets to the hot-deformed ones, and then to sintered ones. As shown in figure 1(b), N_{eff} appears to be more susceptible to the preparation process than a. The significant change of $N_{eff}M_s$ in equation (1) should be primarily responsible for the thermal degradation of H_c. Thus, minimizing local stray fields may be an effective strategy to improve the coercivity thermal-stability.

Considering various microstructural factors involved in both a and N_{eff}, it's of great significance to make clear the decisive influence of microstructure on β. One of the important microstructural factors is grain size. Numerous experiments have shown that H_c generally decreases logarithmically as grain size increases [31–34]. Micromagnetic simulations have well explained the experimental observation, and demonstrate the magnetostatic effects of polyhedral magnetic grains play a key role in the reduction of H_c. The local demagnetizing field calculated on the edge of grain increases linearly with the logarithm of grain size, and N_{eff} can be expressed as [35, 36]:

$$N_{eff}(D) = n \ln\left(\frac{D}{\delta_B}\right) \tag{7}$$

where n depends on the grain shape and the degree of alignment, δ_B represents the magnetic domain wall width and D is the grain size. Thus,

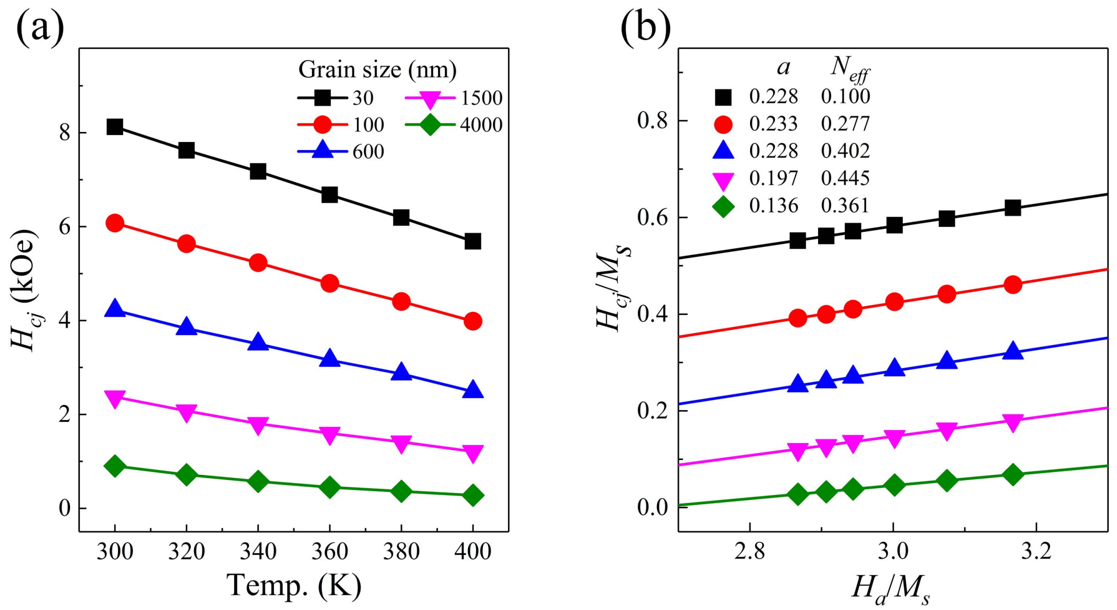

Figure 2. (a) H_c versus temperature and (b) H_c/M_s versus H_a/M_s for different grain-sized $MM_{13.5}Fe_{79.5}B_7$ melt-spun and sintered (green color) magnets.

$$\beta(D) = h + \frac{h - m}{\frac{ak}{n} \cdot \frac{1}{\ln\left(\frac{D}{\delta_B}\right)} - 1} \tag{8}$$

To study the effect of grain size on β, we fabricate $MM_2Fe_{14}B$ melt-spun ribbons with different grain sizes by controlling the spinning speed [37]. The average grain size of $MM_{13.5}Fe_{79.5}B_7$ ribbons at the speed of 5 m/s, 10 m s^{-1}, 15 m s^{-1} and 20 m s^{-1} is about 30 nm, 100 nm, 600 nm and 1500 nm, respectively. Furthermore, we select a $MM_2Fe_{14}B$ sintered magnet with a larger grain size of about 4 μm in this study (the preparation details are available in [38]). The temperature dependence of H_c for all samples are shown in figure 2(a). Then by linear fit of H_c/M_s versus H_a/M_s plot (figure 2(b)), the microstructural parameters a and N_{eff} can be obtained and are shown in the same figure. While a change little, N_{eff} show a logarithmic raise with grain size increasing. However, as the microstructure of high La-Ce content magnet is susceptible to deterioration during high temperature sintering, the $MM_2Fe_{14}B$ sintered magnet suffers from poor control of ideal microstructure having low values for both a and N_{eff}. β of all samples with the corresponding grain sizes are plotted in figure 3. It is found that β drops dramatically with D when it is smaller than about 500 nm and then decreases almost linearly with grain size increasing. A theoretical curve based on equation (8) in red dashed line agrees pretty well with the result. But the $MM_2Fe_{14}B$ sintered magnet exhibits a lower β below the curve due to its poor microstructure. Part of the data in figure 1 for $Nd_2Fe_{14}B$ magnets with the same a are also plotted in figure 3 and a similar downward trend is obtained. The strong dependence of β on grain size well explains the results in figure 1.

In addition, as shown in figure 3, β of $MM_2Fe_{14}B$ and $Nd_2Fe_{14}B$ magnets show different decline rates with grain size due to their different intrinsic magnetic properties (table 1). Especially when D exceeds 1.0 μm, β of $MM_2Fe_{14}B$ magnets with a lower k value decreases faster than that of $Nd_2Fe_{14}B$. The two β(D) curves thereby intersect at about $D = 4.2$ μm. After the intersection point, β of $MM_2Fe_{14}B$ magnets will always be lower than that of $Nd_2Fe_{14}B$. The micron scale grains are more likely to deteriorate the coercivity thermal-stability in $MM_2Fe_{14}B$ magnets compare to $Nd_2Fe_{14}B$. Thus, more effort is needed to refine the grains in the preparation of LaCe-containing sintered magnets to avoid the rapid deterioration of β.

Another key microstructural factor is grain boundary [34, 39]. Depending on thickness and magnetic property, grain boundaries may be act as nucleation of reversal magnetic domains or pinning points impeding domain wall motion, which determines the magnetization reversal mechanism. For the melt-spun magnets with a very thin ferromagnetic rare-earth-rich layer surrounding the nanosized grains [39, 40], intergranular exchange coupling actually plays an important role in determining H_c. Figure 4(a) shows the 300 K demagnetization curves and the corresponding first-order differential curves of $MM_xFe_{94-x}B_6$ melt-spun ribbons ($x = 12, 13, 14, 15, 16, 19$). With the increase of MM from $x = 12$ to $x = 19$, the non-uniform magnetization reversal behavior is increasingly evident and H_c is increased from 4.6 kOe to 9.6 kOe. Grain boundary can be thickened by increasing rare-earth content and accordingly the intergranular exchange coupling would be weakened [28, 40]. Because the magnetization reversal in nanocrystalline magnet is strongly

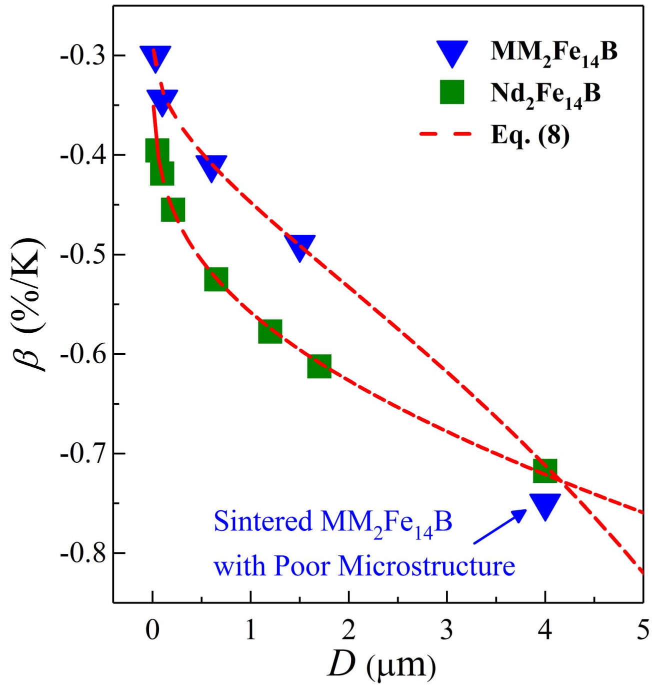

Figure 3. β versus grain size (D) for $MM_2Fe_{14}B$ and $Nd_2Fe_{14}B$ (in figure 1) magnets with their corresponding fitting curves using equation (8).

dependent on the intergranular exchange coupling [41, 42], the increase of H_c is attributed to the nonuniform magnetization reversal process.

Figure 4(b) is the temperature dependence of H_c for $MM_xFe_{94-x}B_6$ melt-spun ribbons (x = 12, 13, 14, 15, 16, 19), and the fitting curves of H_c/M_s versus H_a/M_s plot with the corresponding a and N_{eff} are shown in figure 4(c). The microstructural parameter a for nanocrystalline magnet can be expressed as a modified form of $a = a_k \cdot a_\varphi \cdot a_{ex}$ [18], in which, a_k still reflects the effect of grain surface defect on the crystal anisotropy. a_φ is related to the grain orientation distribution, and a_{ex} represents the influence of intergranular exchange coupling which increases with the exchanged interaction weakening and is equal to one for decoupled magnet. Hence, as exchange coupled magnets turning to magnetically isolated ones by adding MM content, a shown in figure 4(d) increases from 0.11 and 0.49. Meanwhile, N_{eff} also shows an increasing trend from 0.02 to 0.83. Although a is increased, the faster rise of N_{eff} leads to a reduction in a/N_{eff}. Correspondingly, β of $MM_xFe_{94-x}B_6$ ribbons drops from −0.3%/K to −0.4%/K (figure 4(d)). The dependence of β on rare-earth content in nanocrystalline magnets indicates that the enhancement of intergranular exchange coupling is beneficial to the improvement of coercivity thermal-stability.

The thermal-stability of permanent magnet is a comprehensive issue. Magnets based on 2:14:1 structure are usually replaced by Co to improve the temperature coefficient of remanence (α). Figure 5(a) is the temperature dependences of M_s and H_c in $MM_{13.5}Fe_{79.5-y}Co_yB_7$ (y = 3, 6, 9, 12, 15) melt-spun ribbons. The corresponding temperature coefficients m and β as well as the concerned α are shown in figure 5(c). By incorporating Co in the alloy, the Curie temperature (T_C) of $MM_{13.5}Fe_{79.5-y}Co_yB_7$ (y = 3, 6, 9, 12, 15) ribbons is increased from 503 K at y = 0 to 547 K, 588 K, 625 K, 656 K and 681 K, respectively (average +11.8 K to T_C per 1 at% Co substitution). As a result of the enhanced T_C, m and α is greatly improved. But β drops from −0.3%/K to −0.338%/K.

To make clear the negative influences of Co substitution on β, we need to analyze the effect of each variable in equation (4). Firstly, H_a of $Nd_2(Fe_{1-x}Co_x)_{14}B$ (x < 0.38) have been reported to be almost independent of Co content in a temperature range between 300 and 500 K due to the planar anisotropy of Co and the weaker R-Co interactions than R-Fe [5, 43], thus a small amount of Co addition (<0.19 of the total FeCo in this work) in $MM_2Fe_{14}B$ can be reasonably considered to have little effect on H_a and h within the studied temperature range (300–400 K). The variations of k then could be negligible because of the little changes in M_s(300 K) shown in figure 5(a). Secondly, the microstructural parameters of all samples are shown in figure 5(b) that a and N_{eff} are almost unchanged until y = 12; but N_{eff} increases greatly at y = 15. The microstructural analysis using TEM can further confirm this result (figure 6): Co additions (y < 12) hardly affect the microstructure of the substituted magnets, which all have relatively homogeneous nanostructures with average grain size around 30 nm. But inhomogeneous and coarse grains appear in the sample of y = 15 leading to the relatively large N_{eff} value. Therefore the influences of h, k and a/N_{eff} on β can be neglected until y increased to 12. Only m has a great

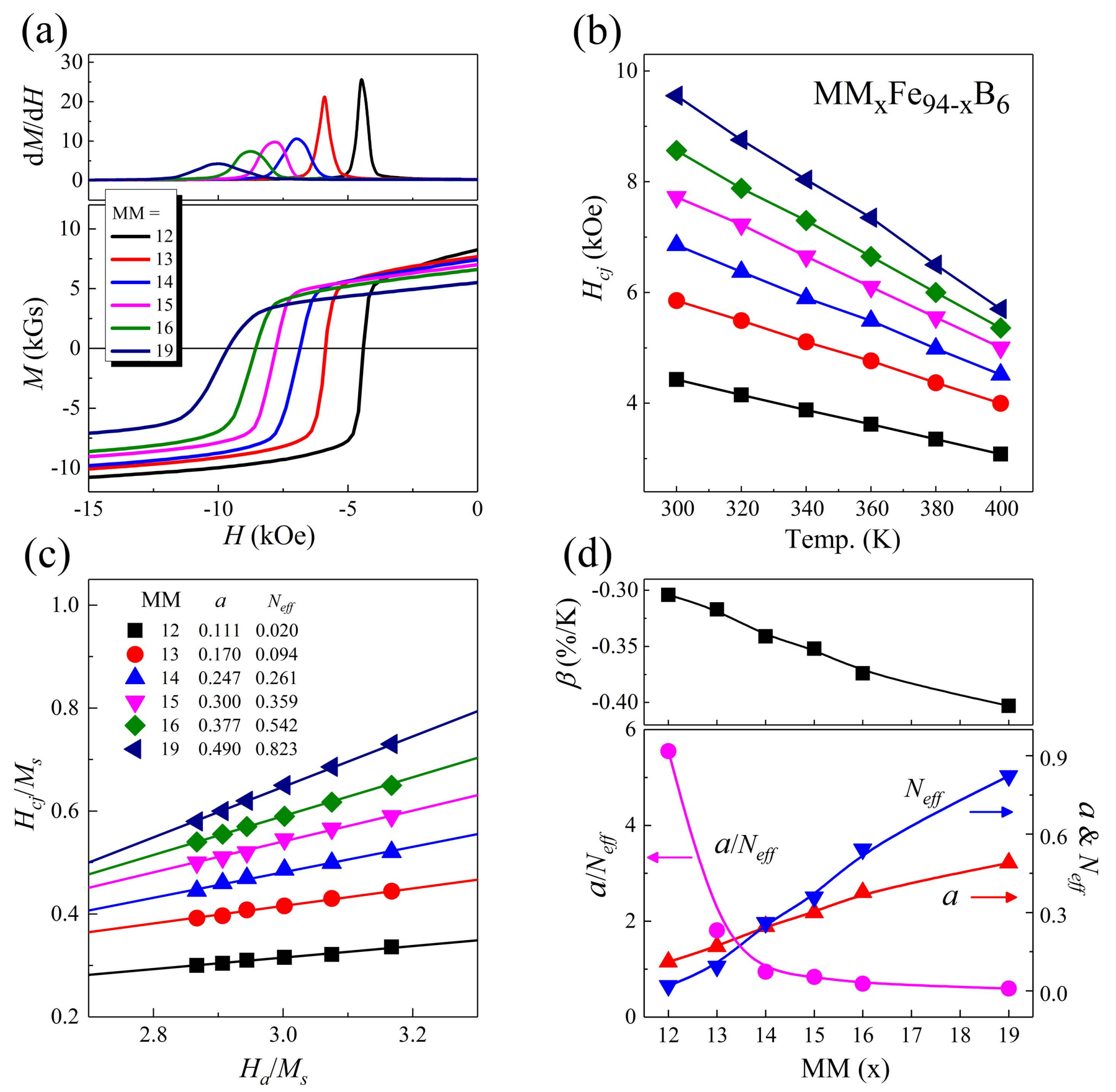

Figure 4. (a) Demagnetization curves and the corresponding first-order derivative curves, (b) H_c versus temperature, (c) H_c/M_s versus H_a/M_s, and (d) β, a, N_{eff} and a/N_{eff} for $MM_xFe_{94-x}B_6$ melt-spun ribbons (x = 12, 13, 14, 15, 16, 19).

impact on β. The relationship between β and m can be simply expressed as: $\beta \sim -m$. As shown in figure 5(c), the linear rise of m with Co content leads to a linear decrease of β before y = 12. However, β of the $MM_{13.5}Fe_{62.5}Co_{15}B_7$ ribbons having relatively large grain sizes is below the linear fit. Nevertheless, owing to very low N_{eff} in exchange coupled magnets, the Co-doped ribbons show small reductions in β. Δ of the $MM_{13.5}Fe_{67.5}Co_{12}B_7$ ribbons is only less than 9%. It implies that enhancing the intergranular exchange coupling is capable of suppressing the deterioration of coercivity thermal-stability caused by Co addition.

4. Conclusions

The dependences of β on the intrinsic magnetic properties and the microstructure of magnets have been established from an extended version of the micromagnetic equation ($H_c = aH_a$-$N_{eff}M_s$). It is straightforward to find out the influencing factors and estimate their respective influence extents through the formula (equation (4)). Based on the analysis of the influences of grain size, MM content and Co substitution on β in MM-Fe-Co-B melt-spun ribbons, the thermal degradation of H_c caused by local stray fields is found to be the dominant factor decreasing the value of β. The research provides an instruction to the enhancement of β in 2:14:1 structure magnets, that is, β can be improved by reducing grain size or rare-earth content. It is expected to serve as a reference for designing and preparing the permanent magnets with high coercivity thermal-stability.

In addition, the temperature range (T_0 = 300 K, T_1 = 400 K) studied in this work is relatively far away from T_C and H_c decreases almost linearly as temperature rises. The analysis and conclusions in this paper are applicable for other temperature ranges (e.g. T_1 = 380 K or T_1 = 420 K) where $H_c(T)$ still varies linearly. As T_1

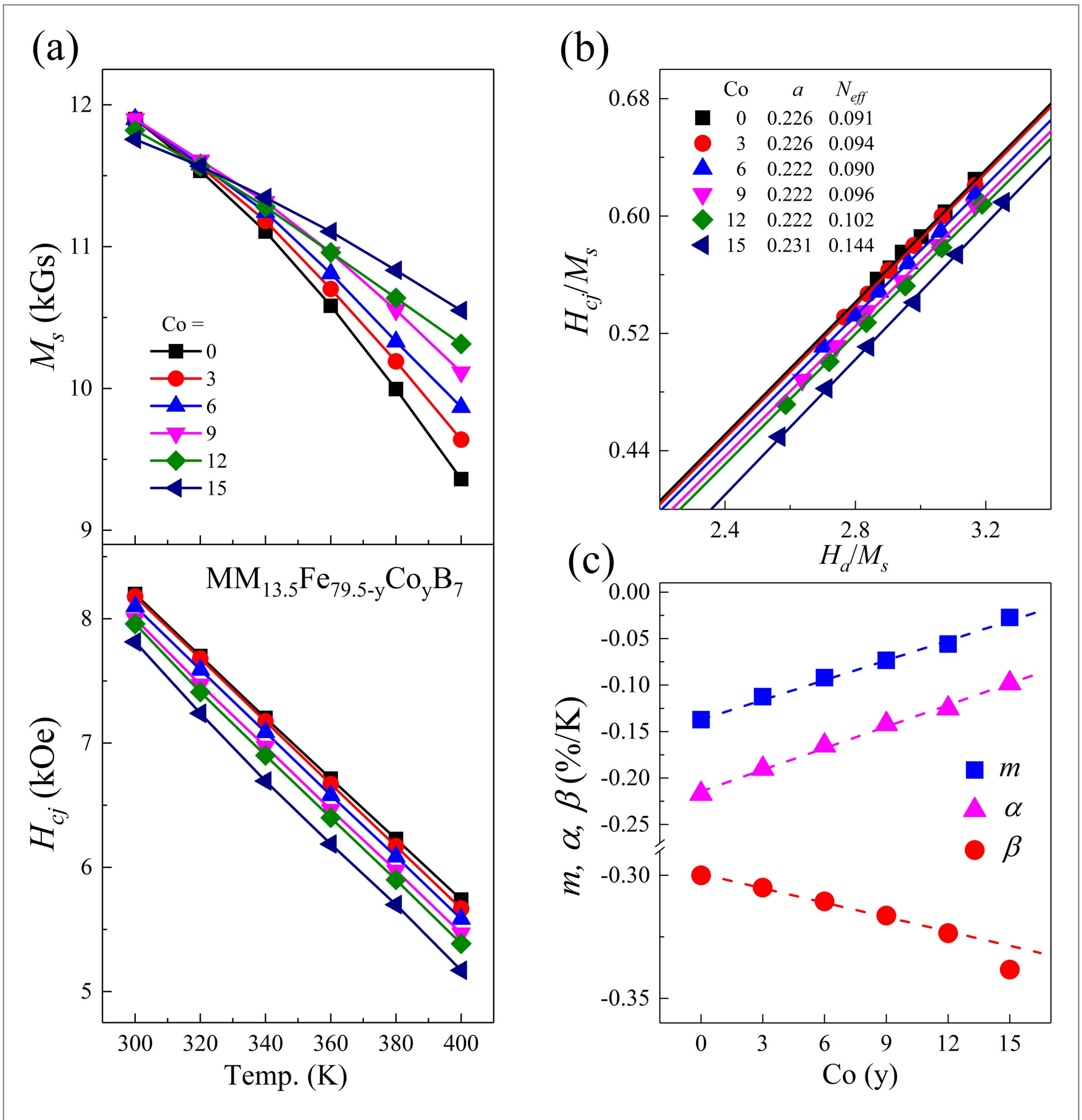

Figure 5. (a) M_s and H_c versus temperature, (b) H_c/M_s versus H_a/M_s, (c) m, α and β for $MM_{13.5}Fe_{79.5-y}Co_yB_7$ melt-spun ribbons (y = 0, 3, 6, 9, 12, 15).

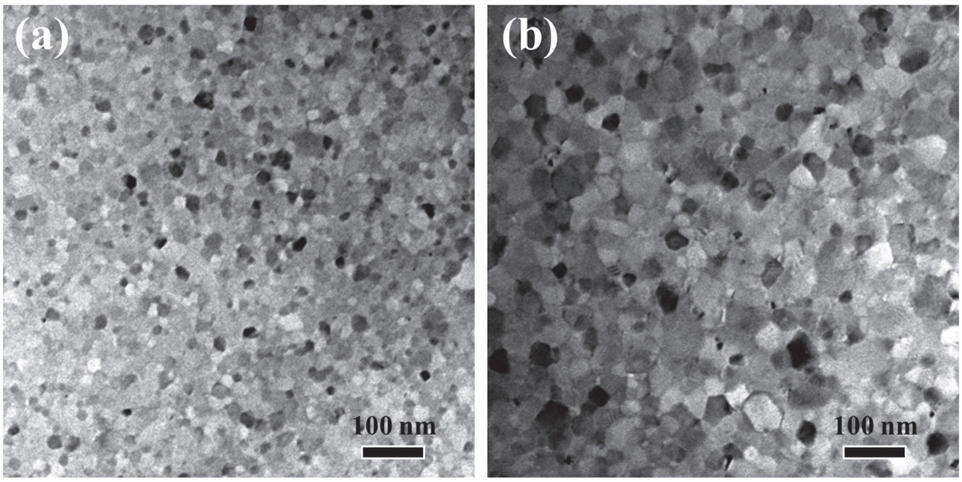

Figure 6. TEM images for $MM_{13.5}Fe_{79.5-y}Co_yB_7$ ribbons of (a) y = 3 and (b) y = 15. Here we only show the images of the sample of y = 3 and y = 15, because the results at y = 0, 6, 9 and 12 are almost the same as y = 3.

further increases, however, the decline of H_c will gradually deviate from the linear. Further investigation on the effect of the nonlinear behaviors in H_c on β should be carried out.

Acknowledgments

This work was supported by the National Basic Research Program of China (Grant No. 2014CB643702), the National Natural Science Foundation of China (Grant No. 51590880), the Knowledge Innovation Project of the Chinese Academy of Sciences (Grant No. KJZD-EW-M05) and the National Key Research and Development Program of China (Grant No. 2016YFB0700903).

ORCID iDs

Rui Li https://orcid.org/0000-0002-8369-1526

References

[1] Jones N 2011 *Nature* **482** 22
[2] Gutfleisch O, Willard M A, Bruck E, Chen C H, Sankar S G and Liu J P 2011 *Adv. Mater.* **23** 821
[3] Brown D N 2016 *IEEE Trans. Magn.* **52** 7
[4] Walmer M S, Chen C H and Walmer M H 2000 *IEEE Trans. Magn.* **36** 5
[5] Sagawa M, Hirosawa S, Tokuhara K, Yamamoto H, Fujimura S, Tsubokawa Y and Shimizu R 1987 *J. Appl. Phys.* **61** 3559
[6] Fan X, Chen K, Guo S, Chen R, Lee D, Yan A and You C 2017 *Appl. Phys. Lett.* **110** 172405
[7] Tang W, Wu Y Q, Dennis K W, Oster N T, Kramer M J, Anderson I E and McCallum R W 2011 *J. Appl. Phys.* **109** 07A704
[8] Yan C, Guo S, Chen L, Chen R, Liu J, Lee D and Yan A 2016 *IEEE Trans. Magn.* **52** 5
[9] Herbst J F 1991 *Rev. Mod. Phys.* **63** 819
[10] Tokunaga M, Kogure H, Endoh M and Harada H 1987 *IEEE Trans. Magn.* **23** 5
[11] Leonowicz M 1990 *J. Magn. Magn. Mater.* **83** 211
[12] Liu Z W, Qian D Y, Zhao L Z, Zheng Z G, Gao X X and Ramanujan R V 2014 *J. Alloys. Compd.* **606** 44
[13] Jiang Q, Zhong M, Quan Q, Zhang J and Zhong Z 2016 *J. Alloys. Compd.* **688** 363
[14] Liu L, Sepehri-Amin H, Ohkubo T, Yano M, Kato A, Sakuma N, Shoji T and Hono K 2017 *Scripta. Mate.* **129** 44
[15] Zhang T, Chen F, Wang J, Zhang L, Zou Z, Wang Z, Lu F and Hu B 2016 *Acta. Mater.* **118** 374
[16] Akiya T, Liu J, Sepehri-Amin H, Ohkubo T, Hioki K, Hattori A and Hono K 2014 *J. Appl. Phys.* **115** 17A766
[17] Lin Z, Han J, Xing M, Liu S, Wu R, Wang C, Zhang Y, Yang Y and Yang J 2012 *Appl. Phys. Lett.* **100** 052409
[18] Goll D and Kronmüller H 2000 *Naturwissenschaften* **87** 423
[19] Scholl R, Elk K and Jahn L 1989 *J. Magn. Magn. Mater.* **82** 235
[20] Kronmüller H 1987 *Phys. Stat. Sol.* **144** 385
[21] Skomski R and Coey J M D 2016 *Scripta. Mater.* **112** 3
[22] Kronmüller H and Durst K D 1988 *J. Magn. Magn. Mater.* **74** 291
[23] Fukada T, Matsuura M, Goto R, Tezuka N, Sugimoto S, Une Y and Sagawa M 2012 *Mater. Trans.* **53** 1967
[24] Liu L, Sepehri-Amin H, Ohkubo T, Yano M, Kato A, Shoji T and Hono K 2016 *J. Alloys. Compd.* **666** 432
[25] Liu J, Sepehri-Amin H, Ohkubo T, Hioki K, Hattori A, Schrefl T and Hono K 2015 *Acta. Mater.* **82** 336
[26] Sepehri-Amin H, Ohkubo T, Nagashima S, Yano M, Shoji T, Kato A, Schrefl T and Hono K 2013 *Acta. Mater.* **61** 6622
[27] Chen Z, Wu Y Q, Kramer M J, Smith B R, Ma B and Huang M 2004 *J. Magn. Magn. Mater.* **268** 105
[28] Sepehri-Amin H, Prabhu D, Hayashi M, Ohkubo T, Hioki K, Hattori A and Hono K 2013 *Scripta. Mater.* **68** 167
[29] Crew D C, Girt E, Suess D, Schrefl T, Krishnan K M, Thomas G and Guilot M 2002 *Phys. Rev.* B **66** 184418
[30] Cui W B, Takahashi Y K and Hono K 2011 *Acta. Mater.* **59** 7768
[31] Li W F, Ohkubo T, Hono K and Sagawa M 2009 *J. Magn. Magn. Mater.* **321** 1100
[32] Uestuener K, Katter M and Rodewald W 2006 *IEEE Trans. Magn.* **42** 10
[33] Ramesh R, Thomas G and Ma B M 1988 *J. Appl. Phys.* **64** 6416
[34] Hono K and Sepehri-Amin H 2012 *Scripta. Mater.* **67** 530
[35] Grönefeld M and Kronmüller H 1989 *J. Magn. Magn. Mater.* **80** 223
[36] Bance S *et al* 2014 *J. Appl. Phys.* **116** 233903
[37] Davies H A and Liu Z W 2005 *J. Magn. Magn. Mater.* **294** 213
[38] Shang R X, Xiong J F, Li R, Zuo W L, Zhang J, Zhao T Y, Chen R J, Sun J R and Shen B G 2017 *AIP Advances* **7** 056215
[39] Toson P, Zickler G A and Fidler J 2016 *Phys. B: Condens. Matter* **486** 142
[40] Liu J, Sepehri-Amin H, Ohkubo T, Hioki K, Hattori A, Schrefl T and Hono K 2013 *Acta. Mater.* **61** 5387
[41] Li Z B, Zhang M, Shen B G and Sun J R 2013 *Appl. Phys. Lett.* **102** 102405
[42] Li Z B, Shen B G, Zhang M, Hu F X and Sun J R 2015 *J. Alloys. Compd.* **628** 325
[43] Hirosawa S, Tokuhara K, Yamamoto H, Fujimura S, Sagawa M and Yamauchi H 1987 *J. Appl. Phys.* **61** 3571